Journal of Microscopy

Journal of Microscopy, Vol. 279, Issue 2 2020, pp. 114–122 doi: 10.1111/jmi.12924
Received 16 December 2019; accepted 18 May 2020

A practical criterion for focusing of unstained cell samples using a digital holographic microscope

R. MALIK*, P. SHARMA†, S. POULOSE*,‡, S. AHLAWAT† & K. KHARE*
*Department of Physics, Indian Institute of Technology Delhi, New Delhi 110016, India
†Phase Laboratories Pvt. Ltd., Technology Based Incubation Unit, Indian Institute of Technology Delhi, New Delhi 110016, India
‡Present address: School of Physics, Trinity College, Dublin 2, Ireland

Key words. Autofocusing, computational imaging, digital holographic microscopy, focusing of transparent objects.

Summary

Digital holographic microscopy (DHM) is an important technique that may be used for quantitative phase imaging of unstained biological cell samples. Since the DHM technology is not commonly used in clinics or bioscience research labs, at present there is no well-accepted focusing criterion for unstained samples that users can follow while recording image plane digital holograms of cells. The usual sharpness metrics that are useful for auto-focusing of stained cells do not work well for unstained cells as there is no amplitude contrast. In this work, we report a practical method for estimating the best focus plane for unstained cells in the digital hologram domain. The method is based on an interesting observation that for the best focus plane the fringe pattern associated with individual unstained cells predominantly shows phase modulation effect in the form of bending of fringes and minimal amplitude modulation. This criterion when applied to unstained red blood cells shows that the central dip in the doughnut-like phase profile of cells is maximal in this plane. The proposed methodology is helpful for standardizing the usage of DHM technology across different users and application development efforts.

Introduction

Digital holographic microscopy (DHM) is an emerging modality used by bio-scientists and pathologists for cell imaging and classification. DHM is an interferometric method where the recorded image data are in the form of an interference pattern between a known reference beam and an object beam that has been transmitted (or reflected) from a cell sample. A temporally coherent illumination like laser is used to derive both the reference and object beams in order to obtain interference fringes with good contrast. The information about the unknown object is embedded in recorded data in the form of amplitude and phase modulation of interference fringes. In DHM, the hologram/interference pattern is recorded on a CCD (Charge Coupled Device) or CMOS (Complementary Metal Oxide Semiconductor) sensor array followed by reconstruction of phase images numerically. An important advantage of DHM is that it can be used to image transparent cell objects that are otherwise difficult to image with typical brightfield microscopes. This is because the cells usually have a natural refractive index contrast with respect to their surroundings and this leads to the phase modulation of interference fringes. At present, quantitative phase as an imaging modality is not very popular among clinical practitioners although its importance has been well established in Optics literature (Park *et al.*, 2018). The main reason for this is that the clinicians are not trained to interpret quantitative phase images of cells. It is therefore important to image the cells in both brightfield mode as well as quantitative phase mode so that the clinical practitioners can correlate the phase images with their years of understanding based on the brightfield microscopy images. A DHM instrument configured to image cells both in usual brightfield as well as quantitative phase modalities (Mangal *et al.*, 2019) has recently been shown to provide valuable diagnostic information for classification of cervical cells. The cervical cells used in that work were stained and therefore fairly easy to focus in the brightfield mode. However, when transparent unstained cells are to be used for DHM-based study, focusing of the cells is not straightforward due to low-amplitude contrast. The aim of this work is to provide a practical criterion for focusing of transparent cell samples directly in the hologram domain. This method can be followed by users while recording a digital hologram or incorporated into a DHM system in the form of an autofocus module. Our method is based on the simple observation that the image plane hologram for focused transparent objects like cells predominantly shows phase (rather than amplitude) modulation of fringes. Based on this criterion, in a typical field of view,

Correspondence to: Kedar Khare, Department of Physics, Indian Institute of Technology Delhi, New Delhi 110016, India. Tel: +91-26591362; E-mail: kedark@physics.iitd.ac.in

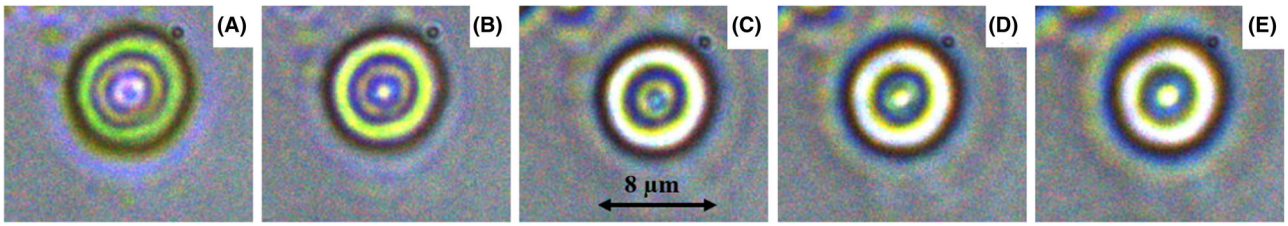

Fig. 1. (A)–(E) Brightfield image of a single RBC in a selected ROI as the microscope focusing stage is translated through the focus plane.

we find that there is often depth variation between different cells leading to distinct phase profiles for same type of cells. This subtle effect can be potentially important when phase-based morphological parameters are used in cell classification studies (Anand *et al.*, 2012).

Numerical autofocusing in digital holography is a well-studied topic in the literature. There are various approaches used for determining the best focus plane which include a method based on a gradient computation and various sharpness metrics (Yu & Cai, 2001; Ilhan *et al.*, 2014). Gillespie & King (1989) use self-entropy of the phase and amplitude as a sharpness metric. Various other metrics such as gradient, variance, Laplacian, deviation-based correlation, autocorrelation, etc., are studied by (Ilhan *et al.*, 2014). Local maximization of the intensity variance is also used as a focus criterion (Ma *et al.*, 2004). Ferraro *et al.* (2003) determine the best focus plane by measuring the phase shift of the hologram fringes. Another method based on maximization of a sharpness metric related to the sparsity of the wavelet (Fresnelet) coefficient has also been proposed (Liebling & Unser, 2004). Dubois *et al.* (2006) use the integral power of the reconstructed object wave amplitude as a focus measure. Implementation of some of these methods on graphical processing unit (GPU) (Dogar *et al.*, 2013) has also been demonstrated for accelerating the computational speed. The autofocusing methods above are based on computation involving propagation of object wavefront from the hologram recording plane to nearby planes and use of focusing criteria on the propagated wavefront (Rinehart *et al.*, 2015). Since our work involves recording of a focused brightfield image as well as hologram of the sample in the same position, the numerical refocusing methods are not directly usable. In particular, the numerical refocusing methods work on the coherent wavefronts but not on the brightfield images that we wish record simultaneously (typically with a white light LED (Light Emitting Diode) illumination). A practical criterion for focusing of transparent samples that is usable while recording the hologram in the laboratory is therefore required.

The present study has been performed with unstained red blood cells (RBCs). In typical pathological examination, RBCs are stained which makes it easier to focus them in the brightfield mode, however, as stated before focusing is not easy when the cells are unstained. In Figs. 1(A)–(E), we show the image of a single RBC when the microscope focusing stage is translated through the focus plane. The microscope is here operated in the brightfield mode and uses white light LED illumination. We observe that since the cells are not stained, determining the exact focus plane is not straightforward. Autofocusing procedures in the brightfield mode typically employ gradient based criteria to detect focus plane. It may be noted that for $\lambda = 650$ nm, the depth-of-focus for the 40× objective used here is nominally given by $\lambda/(2NA^2) = 0.77\,\mu$m and the maximal thickness of RBCs is typically in the range 2–2.5 μm. In Fig. 2, we show the plot of total variation (TV) of a 256×256 region-of-interest (ROI) around the particular RBC. Here, the TV of an image $g(x, y)$ is defined as:

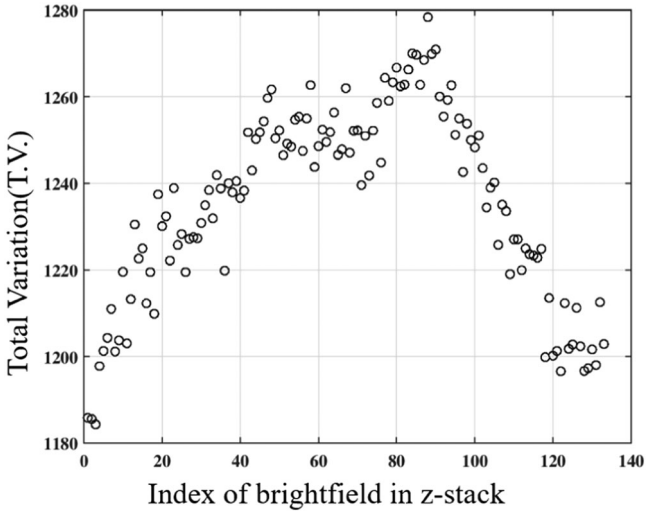

Fig. 2. Gradient-based sharpness measure (total variation) of the brightfield image of unstained RBC in a selected ROI as a function of focus distance. The x-axis index represents index of movie frames recorded, whereas the microscope stage was translated along optic axis by 5 μm.

$$TV(g) = \Sigma_{i=all\,pixels}\sqrt{|\nabla_x g_i|^2 + |\nabla_y g_i|^2}. \quad (1)$$

The brightfield imaging is performed via an afocal imaging system that used a 40× (0.65 NA) infinity corrected objective along with a tube lens of focal length 200 mm. In this experiment, the focus stage was slowly translated along the depth dimension by 5 μm and the camera recorded the images in a movie mode (11 frames per second) so that 132 frames through focus were recorded. A CMOS camera (Model:

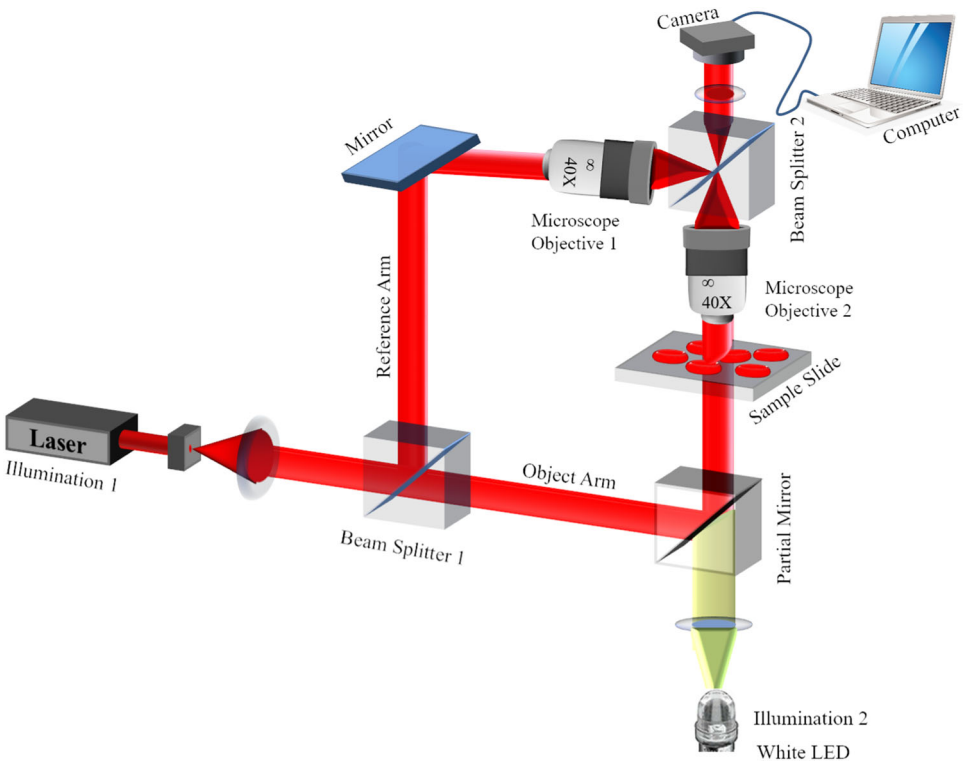

Fig. 3. Schematic of a dual-mode DHM system for recording of a hologram as well a brightfield image of a cell sample by switching the illumination source (laser or white light LED). The interferometer is a balanced Mach–Zehnder system. LED source with a condenser is added such that a brightfield image of the cell sample may be recorded with the sample slide in the same z position. Either laser or LED source is switched on for a given recording.

uEye 3070CP, 2056×1542 pixels of size 3.5 μm; Make: IDS-imaging, Germany) was used for image recording. Based on the frame indices in the movie and the total z-translation, we estimate that the five images shown in Fig. 1 are approximately 1 μm apart on an average. The plot of TV of the ROI around a single unstained RBC shows that there is a broad peak making it difficult to establish the focus plane clearly in an unambiguous way. We therefore decided to observe the digital holograms of the cell ROIs directly. What follows shows some interesting findings that lead to practical focus criterion in the hologram domain. The paper is organized as follows. In section 'Characteristics of holograms of transparent cells recorded through focus region', we describe our observations on the characteristics of holograms of unstained RBC sample as the sample is translated through focus and develop a motivation for amplitude modulation based focus criterion. In section 'Phase reconstructions of a single cell at various defocus positions', the optimization-based phase reconstruction approach we have used in this study is reviewed briefly. In section ''Hologram domain focusing criterion and corresponding phase reconstructions', the hologram domain focusing criterion is applied to a series of through focus holograms of cells. The features in corresponding phase reconstructions of cells are observed carefully to make a case for a uniform focusing method across all DHM-based cell studies. Finally, in the last section, we provide concluding remarks.

Characteristics of holograms of transparent cells recorded through focus region

In the present work, we use a dual-mode DHM system shown in Fig. 3. The system has two illuminations – a low-power diode laser (3 mW, 650 nm) and a white light LED. The balanced Mach–Zehnder interferometer with laser illumination turned on provides the hologram. When the laser is turned off and the white light LED is turned on, the reference arm of the interferometer is not in use and a brightfield image of the sample may be recorded on the camera. Note that both the holographic and the brightfield images may be recorded without disturbing the z-position of the sample slide in this way. For the focus positions shown in Fig. 1(A)–(E), corresponding full field-of-view holograms were separately recorded by switching to the laser illumination. The holograms are shown in Fig. 4(A)–(E). We note that the interference fringes in these recordings in general show both amplitude as well as phase modulation. It is further observed that the cells show an interesting transition in the amplitude modulation from having bright to dark regions around their boundaries.

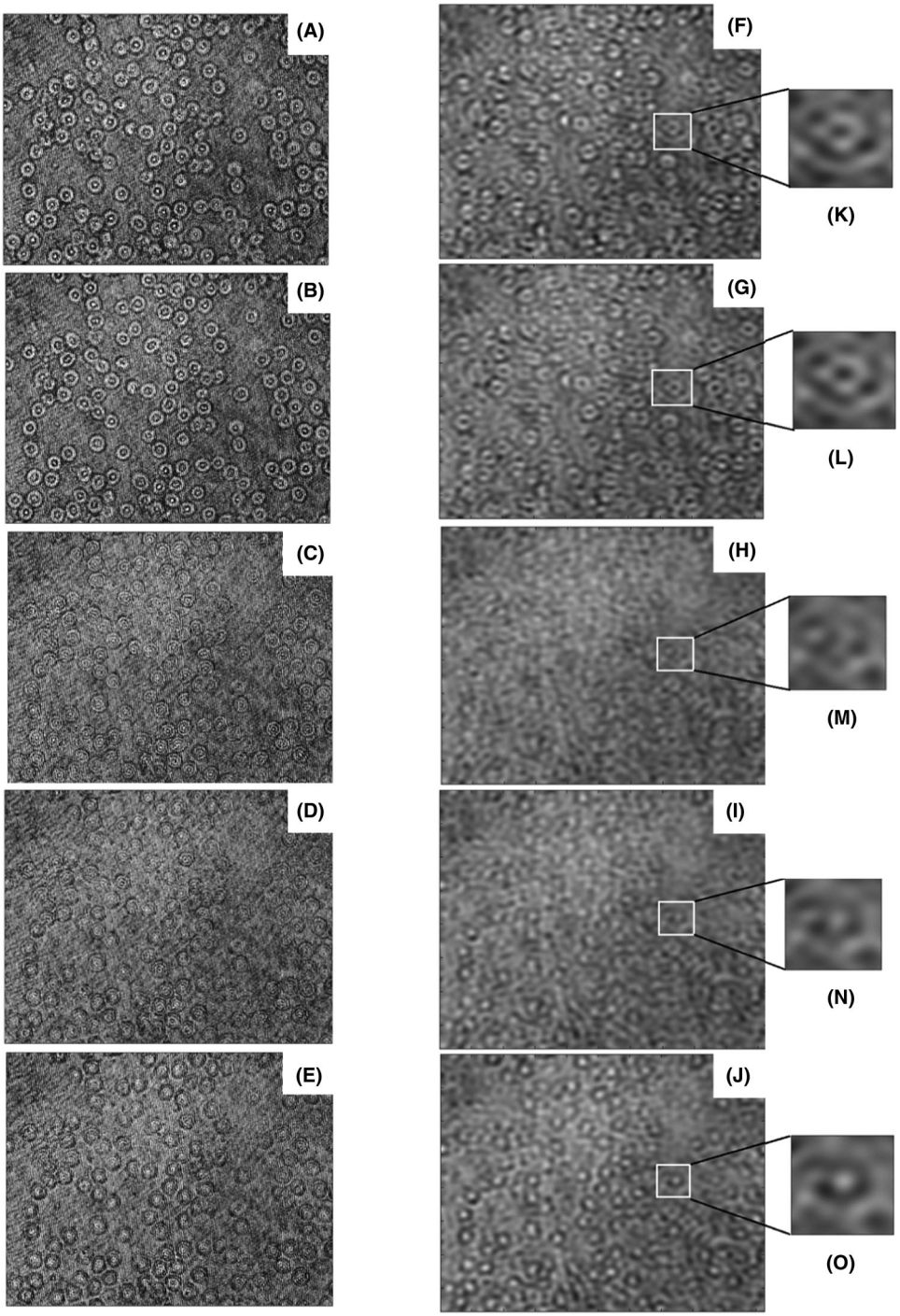

Fig. 4. (A)–(E) Representative holograms H of the blood smear slide as it travels through the focus plane. (F)–(J) Corresponding low-pass-filtered holograms H^{lp}. (K)–(O) Zoomed-in version of selected ROI around the same RBC in the low-pass-filtered holograms.

Holograms in between these extreme stages show minimal amplitude modulation and predominantly have phase modulation (fringe bending) at the location of the cells. We therefore propose that the plane which shows a hologram with minimal amplitude modulation may be treated as the in-focus image plane hologram. The in-focus plane associated with transparent cells can thus be decided manually by visual examination of the fringes or by setting a numerical parameter that can measure the degree of amplitude modulation in the fringes from the recorded hologram images.

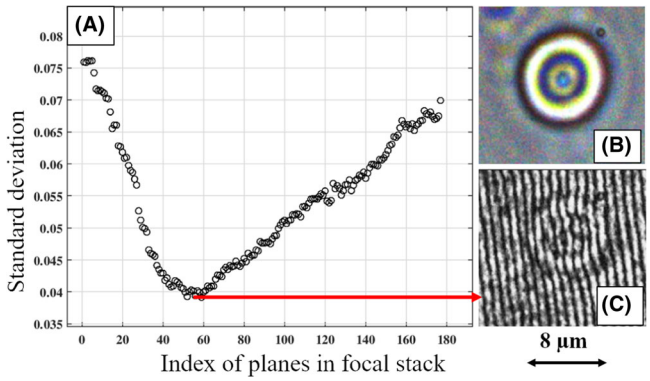

Fig. 5. (A) Standard deviation as a function of the focus distance. (B) Brightfield image at the best focus plane. (C) Hologram at the best focus plane.

To capture the amplitude modulation information in a numerical parameter, the holograms were low-pass-filtered which washes out the fringes as shown for five representative holograms in Figs. 4(F)–(J). Denoting the kth hologram in the hologram stack as $H_k(x, y)$, the low-pass filtering operation may be defined as:

$$H_k^{lp}(x, y) = \mathcal{F}^{-1}\{\mathcal{F}[H_k](f_x, f_y) \cdot L(f_x, f_y)\}. \tag{2}$$

Here $\mathcal{F}$ denotes the 2D Fourier transform operation, (x, y) are the pixel coordinates on the camera and (f_x, f_y) are spatial frequency coordinates in the 2D Fourier transform space. The low-pass filter $L(f_x, L_y)$ is defined as:

$$L(f_x, f_y) = \begin{cases} 1, & \text{for } f_x^2 + f_y^2 <= f_0^2 \\ 0, & \text{otherwise.} \end{cases} \tag{3}$$

The highest frequency f_0 passed by the low-pass filter was selected to be 0.5 times the carrier fringe frequency to make sure that the fringes are not present in the low-pass-filtered holograms H_k^{lp}. The zoomed-out version of ROIs of these low-pass-filtered images are also shown in Figs. 4(K)–(O). We observe that in the transition region where the amplitude modulation changes from bright to dark boundaries around cells, the low-pass ROI images show least fluctuating pixel values. This information can be described by computing the standard deviation of pixel values in the low-pass-filtered images within ROIs of interest. As shown insection 'Hologram domain focusing criterion and corresponding phase reconstructions', the plot of standard deviation for a series of through focus images is clearly able to identify the in-focus plane associated with the transparent cells. In order to further validate this focusing criterion, it is important to observe the phase reconstructions for individual cells in a series of through-focus holograms. Another way of thinking about this criterion is that the plane of minimal amplitude modulation is where the unstained cell can best be approximated as a pure phase object. De-focusing of the holograms causes phase distortion in the phase map of a cell. If DHM-based phase imaging has to become a standard methodology for cell studies, a uniform method for hologram recording and phase reconstruction needs to evolve. Phase map distortions due to defocus are not desirable since they will lead to variability in interpreting the phase images.

Phase reconstructions of a single cell at various defocus positions

In order to further evaluate our focus criterion based on the amplitude modulation of the holograms recorded at different defocus positions, we decided to reconstruct their corresponding phase maps. The phase $\phi(x, y)$ of the wavefront transmitted through the cell sample due to refractive index variation in the cells may be described as:

$$\phi(x, y) = \frac{2\pi}{\lambda} \int n(x, y, z)dz, \tag{4}$$

where $n(x, y, z)$ is the relative refractive index of the cells. There are two traditional phase reconstruction methodologies employed in the literature so far. One is based on Fourier transform method (FTM) (Takeda *et al.*, 1982) and the other one is based on phase shifting method (PSM) (Yamaguchi & Zhang, 1997). FTM is a single-shot method but suffers from poor resolution due to the inherent low-pass filtering nature of numerical processing used. On the other hand, PSM is capable of providing full pixel resolution but is not suitable for field or clinical applications as it has stringent vibration isolation requirements. A third methodology which models the object wave recovery as an optimization problem was proposed in recent years (Khare *et al.*, 2013; Singh *et al.*, 2015; Singh & Khare, 2017) and enables single-shot full-resolution phase reconstruction. If the complex wave scattered from the object in the hologram plane is denoted as $O(x, y)$ and the reference wave is denoted as $R(x, y)$, the mathematical expression for the recorded hologram intensity image $H(x, y)$ is

$$H(x, y) = |O(x, y) + R(x, y)|^2. \tag{5}$$

Optimization-based approach can recover phase information to full detector resolution (Khare *et al.*, 2013) and also offers significant noise advantage (Singh *et al.*, 2015). In optimization method, the recovery of object wave $O(x, y)$ is modelled as a problem of minimizing a cost function of the form:

$$C(O, O^*) = C_1(O, O^*) + C_2(O, O^*), \tag{6}$$

where

$$C_1(O, O^*) = \|H - (|R|^2 + |O|^2 + R^*O + RO^*)\|^2, \tag{7}$$

and

$$C_2(O, O^*) = \sum_{j=all\,pixels} \left[\sqrt{1 + \frac{|\Delta O_j|^2}{\delta^2}} - 1\right]. \tag{8}$$

The first term above is L2-norm squared data fitting term that represents consistency of the object field $O(x, y)$ with the hologram data $H(x, y)$. The second constraint term is the modified

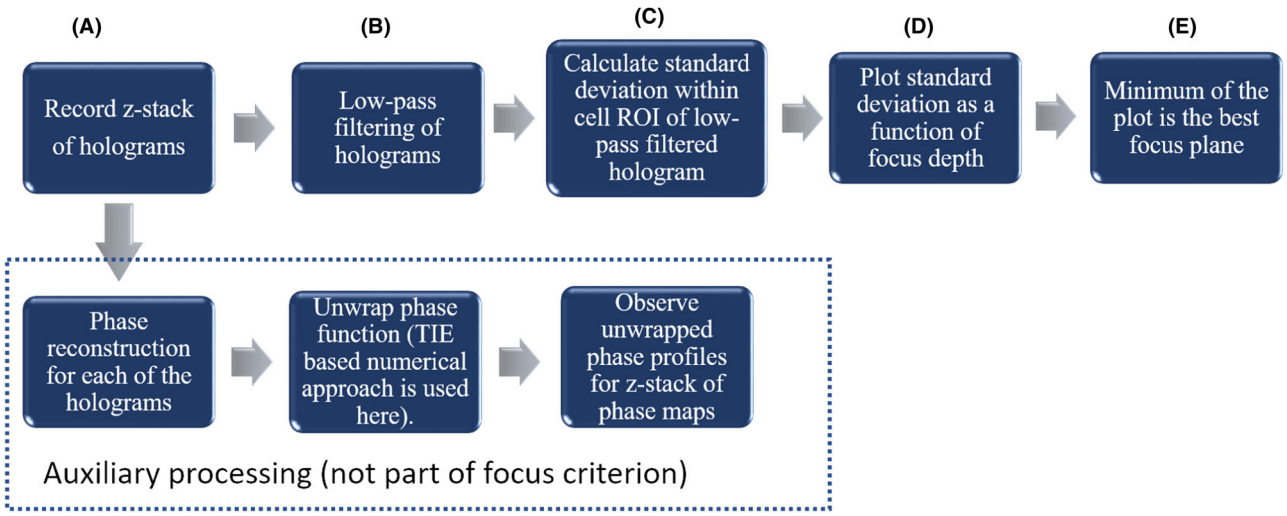

Fig. 6. Flowchart for deciding the best focus plane for unstained cells in hologram domain. The phase reconstruction and unwrapping are auxiliary processing steps that are not part of the focusing criterion and are therefore shown in a dotted box.

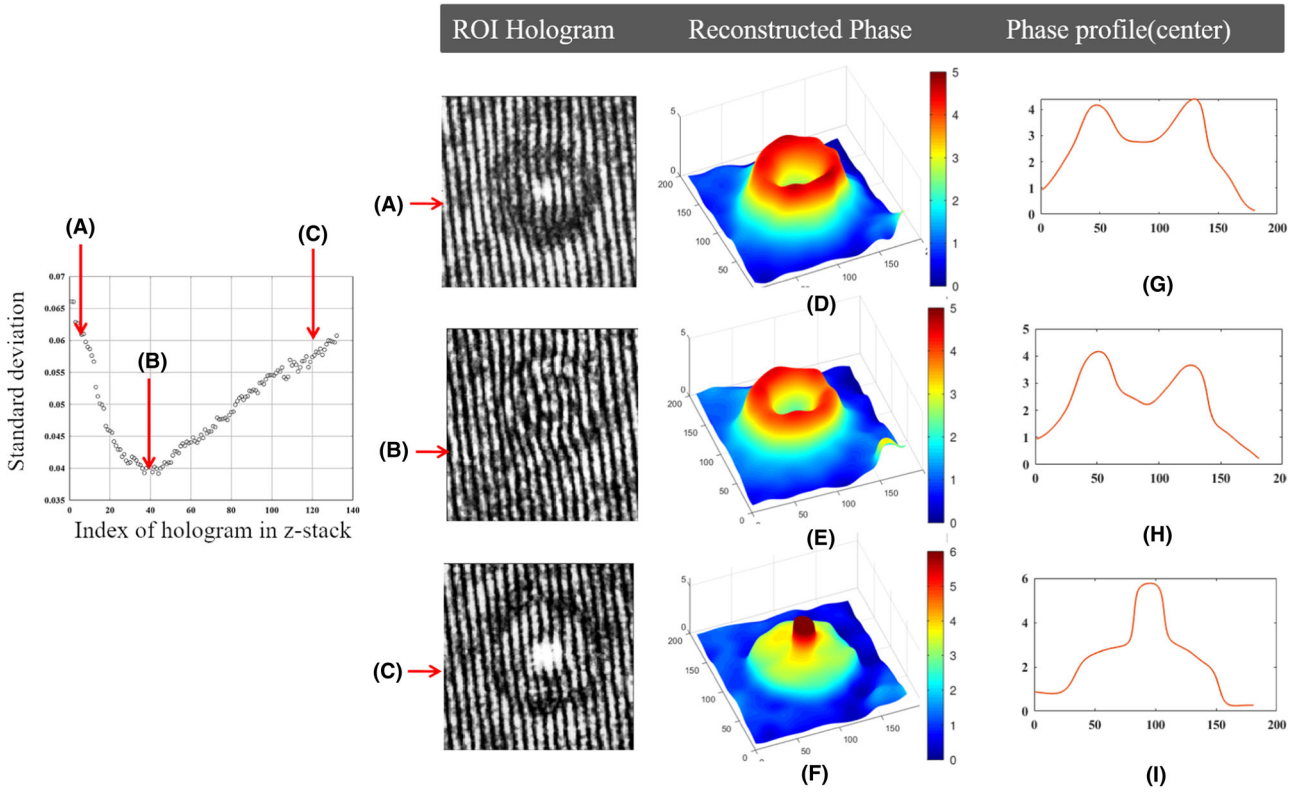

Fig. 7. (A)–(C) Phase map of RBC within selected ROI at different depths from the best focus plane. (A) Below the focus plane, (B) at the best focus plane and (C) above the best focus plane. (D)–(F) show the hologram image at the respective planes and (G)(I) show the profile of RBC phase map through the centre row of the ROI.

Huber penalty. As explained in Mangal *et al.* (2019), the optimization problem in Eq. (6) is solved in an iterative manner. Here, the parameter δ controls the local behaviour of the penalty function. We select δ to be proportional to (1.5 times) the median of gradient magnitudes $|\nabla O_j|$ (j running over all pixels) of the current guess solution. The median represents the most likely gradient magnitude in the image. The pixels with $|\Delta O_j| >> \delta$ may then be associated with edges in the

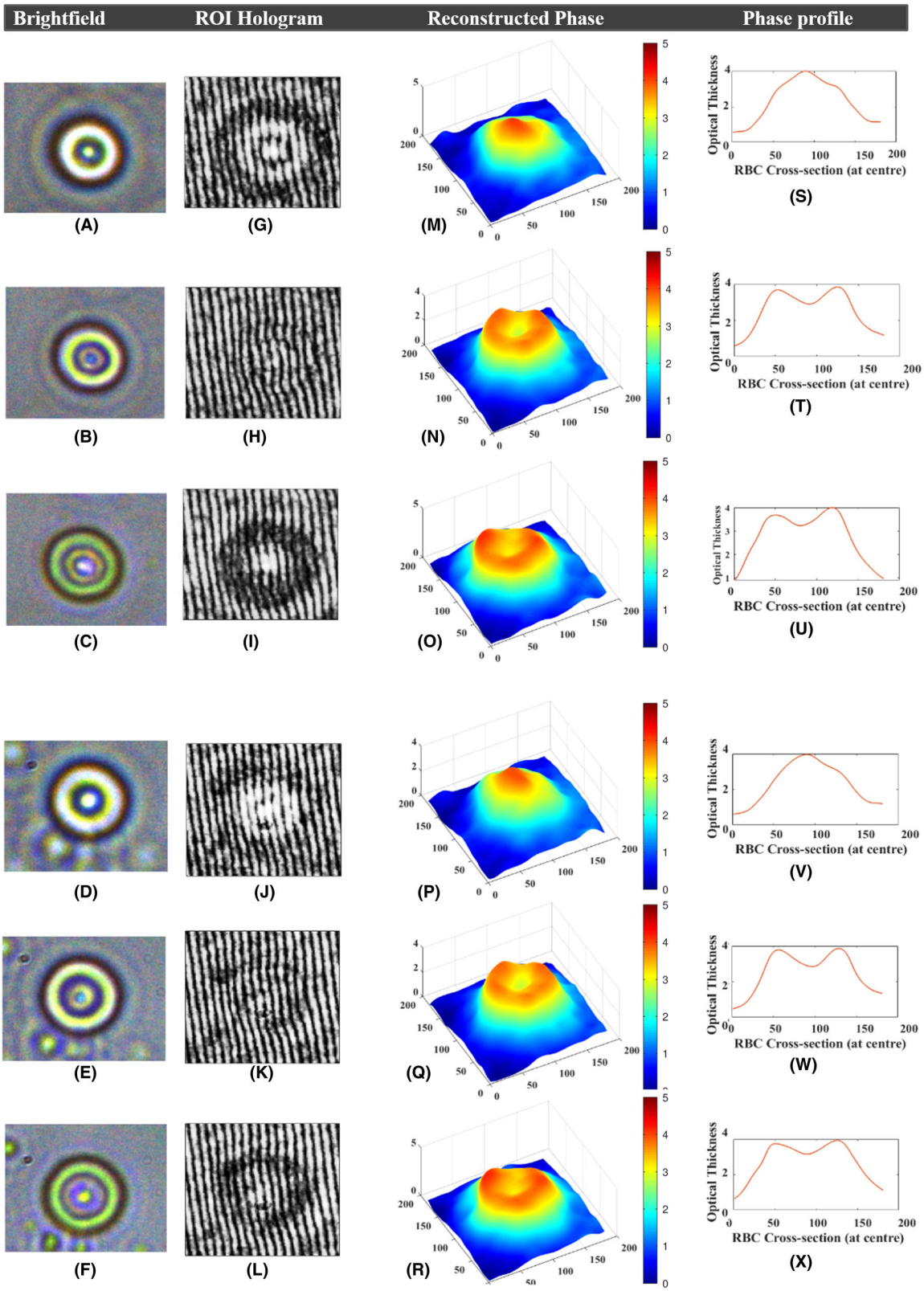

Fig. 8. Illustration of hologram domain focusing criterion for two other RBCs. (A)–(C) and (D)–(F) Brightfield images of two other RBCs at best focus plane and two other planes above and below the best focus plane, (G)–(I) and (J)–(L) corresponding holograms, (M–O) and (P–R) phase reconstructions and (S–U) and (V–X) phase profile plots through RBCs.

image and the penalty act as the TV penalty thereby preserving edge information. The pixels with $|\Delta O_j| << \delta$ represent small local variations and the Huber penalty acts as a smoothing function for these pixels. Thus modified Huber penalty allows us to maintain both the edge as well as smooth grey-level features in the reconstructed phase image of the object.

Since this procedure is performed in the image domain, it allows the reconstruction of the object field $O(x, y)$ over the selected region of interest (Singh & Khare,). In our study, we have used a 256×256 pixel region around a single RBC from a 2056×1542 pixel sized hologram frame to determine the best focus plane of RBC. From the reconstructed complex object field, the phase information $\phi(x, y)$ can be extracted using

$$\phi(x, y) = \arctan\left(\frac{Im[O(x, y)]}{Re[O(x, y)]}\right). \quad (9)$$

This phase is wrapped to the interval $[-\pi, \pi]$ (Malacara, 1992). For unwrapping the phase map, we used transport of intensity-based technique (Pandey *et al.*, 2016) developed in recent years. The reconstruction and unwrapping of the phase profiles were implemented using MATLAB R2018b. We want to emphasize here that the phase reconstruction as described here is not essential for the focusing criterion but has been performed only for understanding the focusing criterion in more detail and correlating it with the phase images of cells.

Hologram domain focusing criterion and corresponding phase reconstructions

In our focusing procedure, we recorded a total of 132 digital holograms of blood smear at different depths across the focus plane using our DHM system with $40\times$ (0.65 NA) infinity-corrected objective. All holograms have the same frame size of 2056×1542 pixels. The amplitude-modulation-based focusing criterion described in section 'Characteristics of holograms of transparent cells recorded through focus region' was implemented with the stack of holograms. The standard deviation in pixel values of the low-pass-filtered versions of holograms computed over 256×256 ROI around a single RBC is plotted in Fig. 5(A). We observe that the standard deviation curve in Fig. 5(A) has a distinct minimum as expected which we associate with the best focus plane. Figs. 5(B) and (C) show the corresponding brightfield image of the RBC and its ROI hologram, respectively. As described above, the ROI hologram at the minimum standard deviation plane is seen to predominantly show phase modulation. The procedure for deciding the best focus plane for unstained cells is summarized in a flowchart in Fig. 6. The optimization methodology described in section 'Phase reconstructions of a single cell at various defocus positions' is used for phase reconstruction of the cell within selected ROI. Figs. 7(A) and (C) show the phase reconstruction away from the focus plane, whereas Fig. 7(B) shows the phase profile for the best focused plane. The standard deviation plot in Fig. 5(A) has been shown again in Fig. 7 for reference. Also for benefit of readers, we would like to state that the ROI holograms shown in Figs. 5(C) and 7(B) are the same. In particular, at the best focus plane as decided by our focusing criterion, we observe that the dip in the centre of the doughnut phase profile is largest. Phase profile in Fig. 7(I) does not even have a doughnut shape. We further note that the change in phase profile of the cell above or below the focus plane is not symmetric (due to aberrations in the objective lens) as is evident from the nature of the corresponding holograms. The size of the phase dip in the centre of the doughnut profile of the RBC phase map has previously been used as a diagnostic marker (Anand *et al.*, 2012). Diagnostic applications using a DHM system typically rely on such morphological parameters derived from the phase images. Any decision-making based on the phase images can therefore be sensitive to the small differences in phase profile due to defocus. Precise focus plane determination while recording an image plane cell hologram using the criterion showed here is therefore critical. In order to further validate our observations, the focusing criterion was applied to multiple RBCs in the sample slide and their corresponding phase reconstructions were studied. Two additional representative examples of cells are shown in Fig 8 where we once again see that the largest central phase dip occurs in the best focus plane as per our criterion.

Conclusion

In conclusion, we have presented a practical method for determination of the best focus plane associated with transparent objects that directly operates in the hologram domain. Unlike traditional autofocusing methods, which rely on numerically propagating the object wave to various distances, this approach allows users to directly record in-focus image plane holograms. This method has other important advantage that once the focus plane is decided in the hologram domain, a focused brightfield image of the sample can also be recorded if required simply by switching the illumination. The method is validated with unstained RBC sample and shows that at the best focus plane, the phase profile of the RBCs shows the highest central dip. It is also observed that small defocus can actually distort the phase map associated with a cell. The method presented here is therefore important for standardization of DHM-based imaging for diagnostic applications or basic cell biology research. The simplicity of our methodology means that this idea can be used for designing an autofocusing tool for DHM systems used for imaging of unstained cell samples.

Acknowledgements

Partial support from following sources is acknowledged: Department of Biotechnology, Ministry of Science and Technology, Grant/Award Number: BT/SBIRI1457/33/16; Department of Science and Technology, Ministry of Science

and Technology, Grant/Award Number: ID/MED/34/2016, BIRAC-SRISTI, Grant/Award Number: GYTI-2017.

References

Anand, A., Chhaniwal, V.K., Patel, N.R. & Javidi, B. (2012) Automatic identification of malaria-infected rbc with digital holographic microscopy using correlation algorithms. *IEEE Photon. J.* **4**(5), 1456–1464.

Dogar, M., Ilhan, H.A. & Ozcan, M. (2013) Real time auto-focusing digital holographic microscope using graphics processors. *Rev. Sci. Instrum.* **84**, 083704.

Dubois, F., Schockaert, C., Callens, N. & Yourassowsky, C. (2006) Focus plane detection criteria in digital holographic microscopy by amplitude analysis. *Opt. Exp.* **14**, 5895–5908.

Ferraro, P., Coppola, G., Nicola, S.D., Finizio, A. & Pierattini, G. (2003) Digital holographic microscope with automatic focus tracking by detecting sample displacement in real time. *Opt. Lett.* **28**, 1257–1259.

Gillespie, J. & King, R.A. (1989) The use of self-entropy as a focus measure in digital holography. *Pattern Recognit. Lett.* **9**, 19–25.

Ilhan, H.A., Dogar, M. & Ozcan, M. (2014) Digital holographic microscopy and focusing methods based on image sharpness. *J. Microsc.* **225**, 138–149.

Khare, K., Samsheerali, P.T. & Joseph, J. (2013) Single shot high resolution digital holography. *Opt. Exp.* **21**, 2581–2591.

Liebling, M. & Unser, M. (2004) Autofocus for digital Fresnel holograms by use of a Fresnelet-sparsity criterion. *J. Opt. Soc. Am. A* **21**, 2424–2430.

Ma, L., Wang, H., Li, Y. & Jin, H. (2004) Numerical reconstruction of digital holograms for three-dimensional shape measurement. *J. Opt. A: Pure Appl. Opt.* **6**, 396–400.

Malacara, D. (1992) *Optical Shop Testing*. 2nd edn. Wiley, New York; Chichester.

Mangal, J., Monga, R., Mathur, S.R., Dinda, A.K., Joseph, J., Ahlawat, S. & Khare, K. (2019) Unsupervised organization of cervical cells using bright-field and single-shot digital holographic microscopy. *J. Biophoton.* **12**, e201800409.

Pandey, N., Ghosh, A.G. & Khare, K. (2016) Two-dimensional phase unwrapping using the transport of intensity equation. *Appl. Opt.* **55**, 2418–2425.

Park, Y., Depeursinge, C. & Popescu, G. (2018) Quantitative phase imaging in biomedicine. *Nat. Photon.* **12**, 1749–4893.

Rinehart, M.T., Park, H.S. & Wax, A. (2015) Influence of defocus on quantitative analysis of microscopic objects and individual cells with digital holography. *Biomed. Opt. Exp.* **6**, 2067–2075.

Singh, M. & Khare, K. (2017) Single-shot interferogram analysis for accurate reconstruction of step phase objects. *J. Opt. Soc. Am. A* **34**, 349–355.

Singh, M. & Khare, K. (2018) Single-shot full resolution region-of-interest (ROI) reconstruction in image plane digital holographic microscopy. *J. Mod. Opt.* **65**, 1127–1134.

Singh, M., Khare, K., Jha, A.K., Prabhakar, S. & Singh, R.P. (2015) Accurate multipixel phase measurement with classical-light interferometry. *Phys. Rev. A* **91**, 021801.

Takeda, M., Ina, H. & Kobayashi, S. (1982) Fourier-transform method of fringe-pattern analysis for computer-based topography and interferometry. *J. Opt. Soc. Am.* **72**, 156–160.

Yamaguchi, I. & Zhang, T. (1997) Phase-shifting digital holography. *Opt. Lett.* **22**, 1268–1270.

Yu, L. & Cai, L. (2001) Iterative algorithm with a constraint condition for numerical reconstruction of a three-dimensional object from its hologram. *J. Opt. Soc. Am. A* **18**, 1033–1045.